Available online at www.sciencedirect.com
ScienceDirect
International Journal of Solids and Structures 45 (2008) 1430–1444
INTERNATIONAL JOURNAL OF SOLIDS AND STRUCTURES
www.elsevier.com/locate/ijsolstr

Comparison of ductile fracture properties of aluminum castings: Sand mold vs. metal mold

H. Mae [a,*], X. Teng [b], Y. Bai [b], T. Wierzbicki [b]

[a] 4630 Shimotakanezawa, Haga-machi, Haga-gun, Tochigi 321-3393, Honda R&D Co., Ltd., Japan
[b] Impact & Crashworthiness Lab, Room 5-218, Massachusetts Institute of Technology, Cambridge, MA 02139, USA

Received 9 June 2007; received in revised form 31 August 2007
Available online 30 October 2007

Abstract

This paper compares mechanical properties of two types of cast aluminum components made in sand molds and cast iron molds, respectively. For each type of the castings, a total of 12 fracture tests are performed under a wide range of stress states including 6 tensile tests on notched and unnotched round bars and 6 biaxial loading tests on butterfly specimens. Using a combined experimental–numerical approach, the plasticity and fracture properties of the components are characterized in terms of the true stress–strain curve and the ductile fracture locus. It is found that the sand-molding component is of higher yield resistance and lower ductility than the metal-molding one. Meanwhile, the fractographic study reveals that there exist two competing failure mechanisms: the internal necking of the matrix at high positive stress triaxialities and void sheeting due to shear at negative stress triaxialities. The transition of the failure modes occurs in the intermediate range. This suggests that a ductile fracture locus formulated in the space of the stress triaxiality and the effective fracture strain consist of three branches rather than a monotonic curve.

Keywords: Failure mechanism; Ductile fracture criterion; True stress–strain curve; Cast aluminum alloy; Sand mold; Metal mold

1. Introduction

Sand and metal are two types of mold media commonly used in casting manufacturing processes. Because of superior heat dissipation ability, metal molds are able to rapidly solidify cast alloys and thus to refine dendrite cells. Cast components made in metal molds usually exhibit higher ductility than in sand molds.

The improvement of mechanical properties of aluminum castings by increasing solidification rates was reported in the literature. Cáceres et al. (1995) and Wang (2003) obtained a wide range of solidification rates in one single cast thick plate by attaching a large cast iron chill at one end. Tensile tests were performed on round bars prepared at different distances from the chill. It was shown that the specimen machined at the chilled end was of the largest elongation to fracture. Shabestari and Moemeni (2004) evaluated four different

* Corresponding author. Tel.: +81 28 677 3311; fax: +81 28 677 7500.
E-mail address: Hiroyuki_Mae@n.t.rd.honda.co.jp (H. Mae).

0020-7683/$ - see front matter © 2007 Elsevier Ltd. All rights reserved.
doi:10.1016/j.ijsolstr.2007.10.016

types of molds made of graphite, copper, cast iron, and sand, respectively. It appears that the graphite mold produces the casting of the highest ductility. In these studies, the material ductility was characterized through round bar tensile tests. A previous study reveals that cast aluminum components are of significantly higher resistance to fracture under shear than under tension (Mae et al., 2007). Hence, it would be interesting to study effects of solidification rates on fracture properties under compression and shear.

The ductility is closely related to material microstructure. Metallographic and fractographic analysis provides a deep insight into the failure mechanism of cast aluminum alloys. Powell (1994) found that aluminum castings tended to break by the intergranular fracture mode. By carefully reviewing the fracture surfaces of cast aluminum specimens, Leupp and Epprecht (1977) concluded that crack formation between grains was essentially of the ductile fracture type, though small plastic deformation always presented in tensile tests on cast aluminum components. Using scanning electron microscopes, Cáceres et al. (1995) and Wang (2003) discovered that the failure mechanism changed from the intergranular fracture mode to the transgranular one as the size of dendrite cells increased. Note, that those failure mechanisms were identified, all from tensile tests on round bars. In contrast to the tensile failure mechanism, the fracture mode of cast aluminum alloys under compression and shear is less understood. By observing polished fracture surfaces of high pressure die cast aluminum alloys, Mohr and Treitler (2008) suggested that shear instability would be a dominant failure mode for specimens under compression.

In this study, a systematic comparison of plasticity and fracture properties of cast aluminum components is made between sand molds and metal molds. A total of 24 fracture tests are conducted for the two types of castings including tensile tests on round bars and biaxial loading tests on butterfly specimens. The true stress–strain curve and the fracture locus are calibrated to characterize plasticity and ductility of the castings, and to differentiate effects of the mold media. Meanwhile, a fractographic examination on the specimens is performed to understand microscopic failure mechanisms under a wide range of stress states.

2. Specimen preparation and test procedures

All the specimens in the present paper were prepared from prototype components, see Fig. 1. The thin-walled casting is a part of an automotive chassis system. Since solidification rates vary with the geometrical dimensions and shape of castings, it is of practical interest to use a real product rather than a specifically cast block. The cast aluminum components were made of the A356 aluminum alloy in sand and cast iron molds under gravity pressure, respectively. By contrast, low pressure die casting was used in a previous study (Mae et al., 2007). Table 1 lists the chemical composition of the A356 aluminum alloy. The T6 heat treatment was applied, which is believed to improve the ductility of the castings.

Depending on stress states and loading histories, a material may display different levels of ductility. An early study indicates that cast aluminum components under compression are able to undergo significant plastic deformation without failure while under tension the effective plastic strain to fracture is only a few percentages (Mae

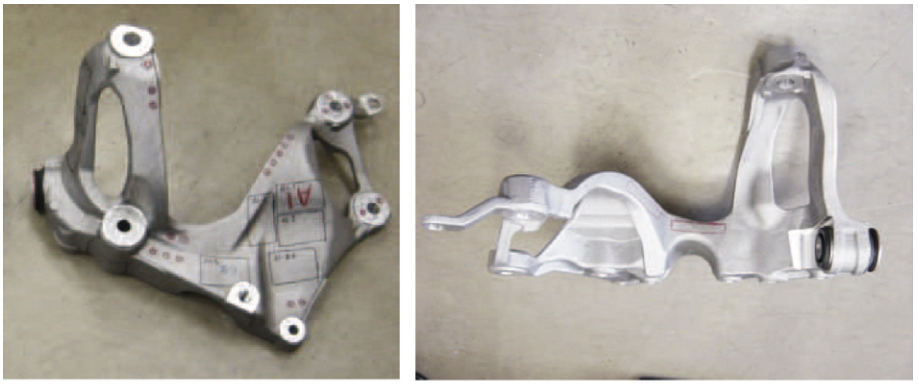

(a) Isometric view (b) Side view

Fig. 1. A cast aluminum component studied in this research. The rectangles and the small circles marked on the exterior surface represent, respectively, the cutting locations of the specimens for the fracture test and of the cylinders for the metallographic study.

Table 1
Chemical composition of the studied cast alloy (wt%)

Cu	Si	Mg	Zn	Fe	Mn	Ni	Ti	Pb	Sn	Cr	Sr
<0.02	6.5–7.5	0.3–0.4	<0.10	<0.20	<0.10	<0.05	<0.20	<0.05	<0.05	<0.05	0.004–0.015

et al., 2007). At the same time, the present casting, though designed to resist compression, may experience complex stress states under accidental loading. This necessitates a full description of the ductility of the cast component under a wide range of loading conditions. In this research, two classes of fracture tests were designed and executed: tensile tests on notched and unnotched round bars, and biaxial loading tests on butterfly specimens.

The tensile tests on round bars are commonly used to calibrate plasticity and fracture properties of materials. Here, three types of round bars including one unnotched and two notched were machined, see Fig. 2. The specimens are of the same minimum diameter of 6.0 mm in the gauge sections and of the same diameter of 9.5 mm in the shoulder parts. The notch radii are $R = 3$ mm and 9 mm, respectively. The notch is introduced to impose a constraint on the deformation of the gauge section. Depending on the radius of the notch, the specimens of the same minimum diameter break at different plastic strains.

The round bar tensile tests characterize the ductility of the cast components under tension. Fracture properties under compression and shear are determined from biaxial loading tests on butterfly specimens. The butterfly specimen is of double curvature in the gauge section and thus there is a smooth transition from the shoulder region to the gauge section. The stress concentration on the boundary of the gauge section is diminished. At the same time, the central region of the gauge section is of the minimal thickness 1.0 mm, which is one third of the thickness of the shoulder region. This design ensures that a macroscopic crack would first occur at the center of the gauge section. The geometrical dimensions of the butterfly specimen are given in Fig. 3.

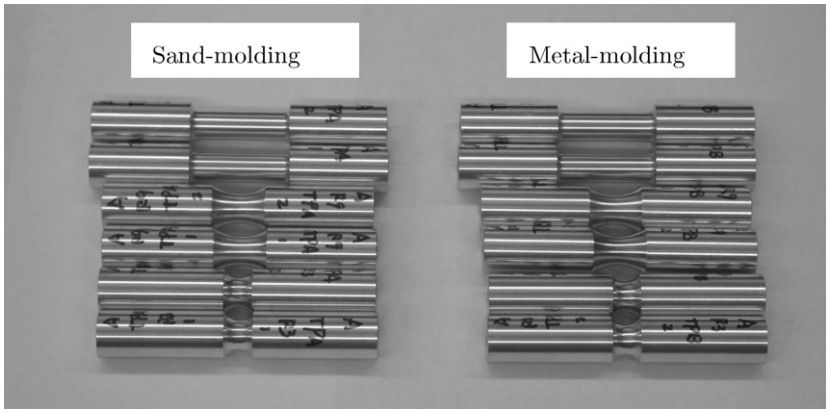

Fig. 2. The unnotched and notched round bar specimens tested in this study.

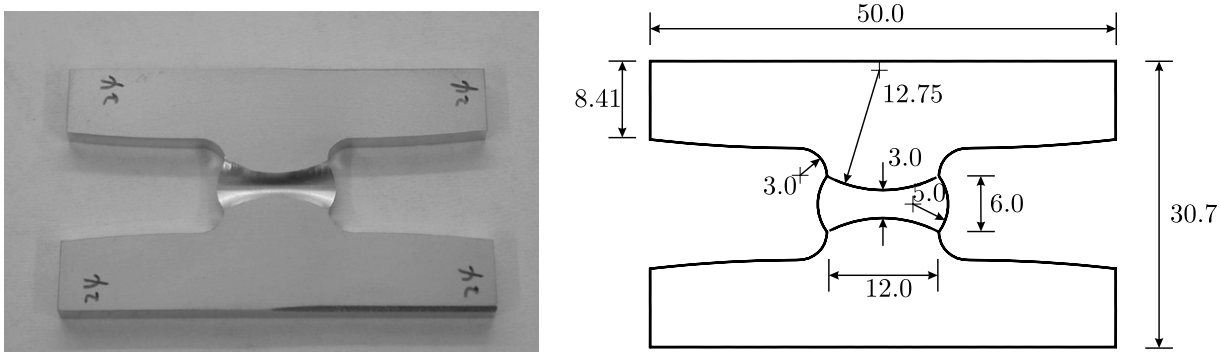

(a) A butterfly specimen (b) Major geometrical dimensions

Fig. 3. Major geometrical dimensions of the butterfly specimen.

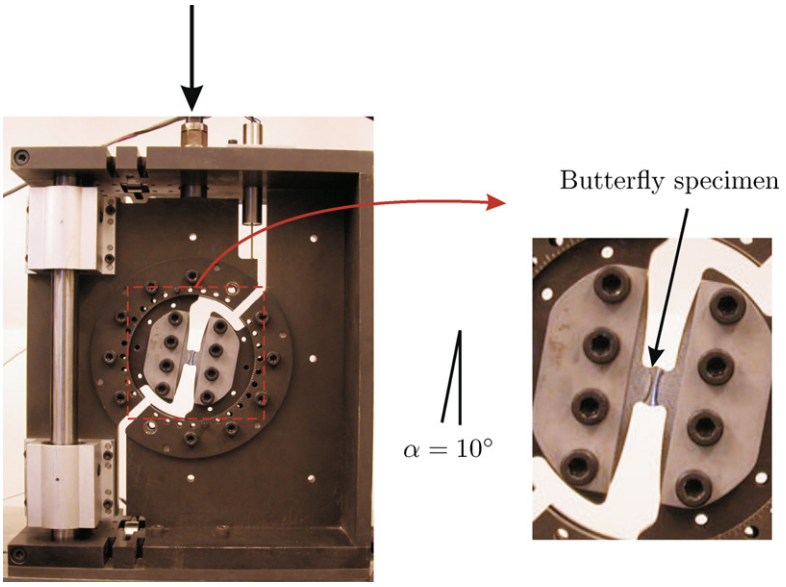

Fig. 4. A butterfly specimen mounted in the Universal Biaxial Testing Device (UBTD) with the inclination angle $\alpha = 10°$ with respect to the loading axis.

The fracture tests on the butterfly specimens were carried out using a custom-made Universal Biaxial Testing Device (UBTD). Fig. 4 shows a butterfly specimen mounted in the UBTD with the inclination angle of 10°. By suitably changing the orientation of the butterfly specimen with respect to the vertical loading axis, various stress states can be generated with different ratios between tension (compression) and shear. With this device one can use one type of specimens to obtain fracture properties under a wide range of stress states. A detailed description of the working mechanism of the UBTD can be found in the paper of Mohr and Doyoyo (2004). The device was first used to investigate the plasticity of aluminum honeycomb under multiaxial loading, and later applied in combination with butterfly specimens to calibrate fracture properties of metals, see Wierzbicki et al. (2005b) and Mohr and Treitler (2008).

In the present research, five biaxial loading conditions were considered from combined compression and shear, pure shear, to combined tension and shear. The inclination angle of the specimens varies from −10°, −5°, 0°, +10°, to +20°. It is expected that the stress triaxialities obtained from these tests would be evenly distributed from −1/3 to +1/3. The two data correspond to uniaxial compression and tension, respectively.

A total of 6 round bars and 6 butterfly specimens were machined from each type of the castings. All the tests were conducted with a universal 200 kN kinematically driven MTS machine at room temperature. The loading velocity was 0.2 mm/min. The vertical reaction force was sampled by a load cell. The deformation process of the specimens was recorded by an optical measurement system, which includes one/two high-speed cameras, a digital photo acquisition device, and a post-processing program. The relative displacement of two arbitrary points on the exterior surface of specimens can be calculated from images captured by the cameras. The optical displacement and the MTS load measurement systems are synchronized and thus the relationship between the load and the displacement can be easily established. The tests also provide the critical displacement to fracture.

3. Microscopic observations

3.1. Microstructure

This section presents metallographic and fractographic examinations of the two types of the cast aluminum components. In order to evaluate effects of mold media on the microstructure of the castings, dozens of small

cylinders were prepared and polished for microscopic observation and measurement. Two selected SEM graphs are displayed in Fig. 5 showing typical aluminum-rich dendrites separated by eutectic regions. The Secondary Dendrite Arm Spacing (SDAS) was measured to describe the microstructure. The average values of the SDAS are 60 μm and 40 μm, respectively, for the sand-molding and the metal-molding components. The increase in the cooling rate refines dendrite cells and silicon particles in eutectic regions. This result is consistent with the findings in the literature, e.g. see Cáceres et al. (1995) and Wang (2003).

3.2. Fractographic analysis

To better understand the failure mechanism of the castings under various loading conditions, the fracture surface of each specimen was examined with a scanning electronic microscope. Some of the SEM pictures are selectively presented in the paper. Fig. 6 shows the fractographs of the unnotched round bars. A number of small dimples, which is a typical characteristic of the ductile fracture, can be easily recognized. The fracture surfaces also exhibit many, smooth, flat areas separated by bright ridges. The flat areas are cleaved silicon particles. Studies have found that the fracture of cast aluminum alloys is often initiated by the cracking of silicon particles, e.g. see Dighe et al. (2002) and Wang (2003). The occurrence of the bright ridges indicates that voids/microcracks could link by the necking of the matrix. The butterfly specimens under the combined tension and shear loading with $\alpha = 20°$ display a similar microscopic fracture pattern to the round bars, see Fig. 7. Although a shear stress component is active, dimples do not appear to grow along a preferential direction.

The specimens under tension mainly fail by the intergranular fracture mode, i.e. the fracture surfaces of the specimens are formed as the cracks grow along grain boundaries. This is readily discernable from a low magnification SEM fractograph, see Fig. 8.

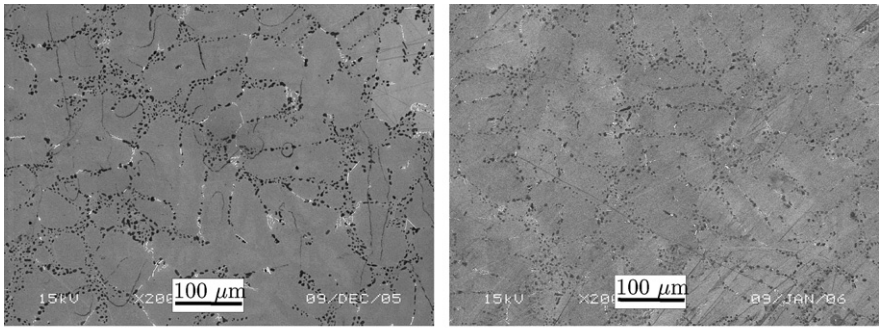

Fig. 5. Microscopic structures of the sand-molding and the metal-molding components.

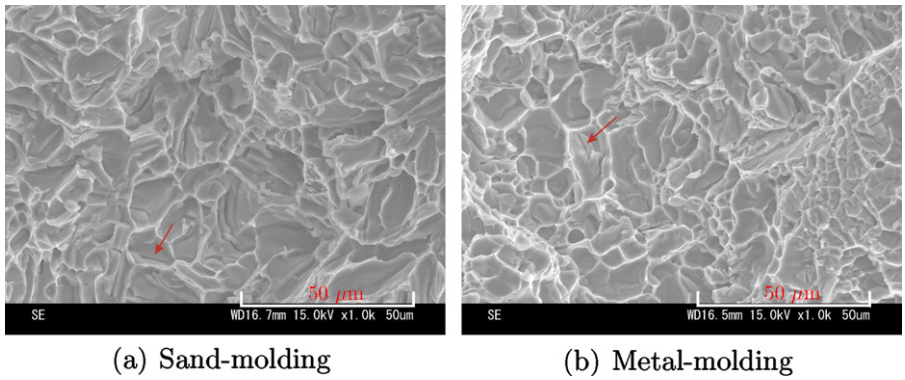

Fig. 6. Fractographs of the tensile tests on the unnotched round bars. The arrows indicate the cracked silicon particles.

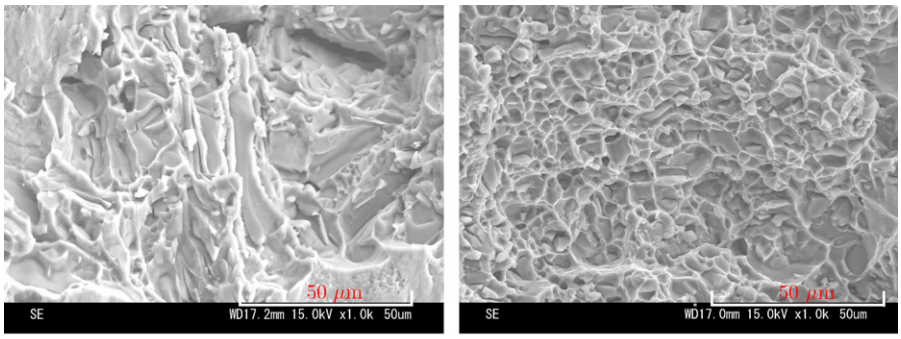

(a) Sand-molding (b) Metal-molding

Fig. 7. Fractographs of the combined tension and shear tests on the butterfly specimens with $\alpha = +20°$.

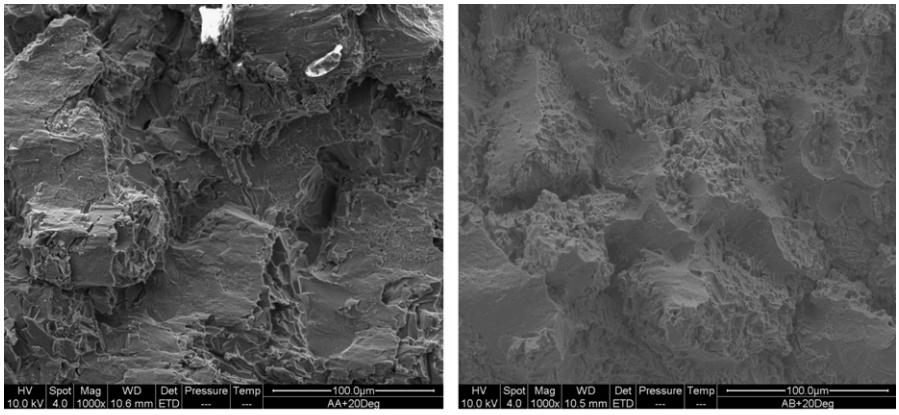

(a) Sand-molding (b) Metal-molding

Fig. 8. Low magnitude fractographs of the combined tension and shear tests on the butterfly specimens with $\alpha = +20°$.

As the ratio of shear to tension increases, the elongation of the dimples along the shear direction becomes evident, see Fig. 9 for the case with $\alpha = 10°$. This corresponds to the transition of the mode of void coalescence from internal necking to void sheeting. As suggested by Rogers (1960) and Hancock and Mackenzie (1976), internal necking and void sheeting are two competing mechanisms for void linkage. At low stress triaxialities, void sheeting is a preferable mode. Similar fracture patterns were observed in tensile tests on round bars super-

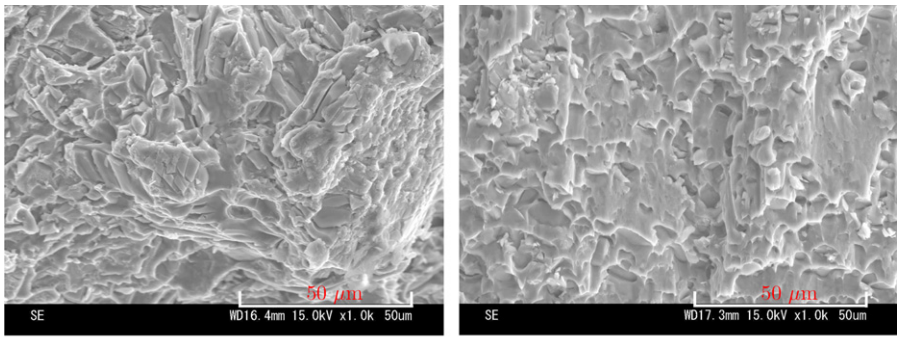

(a) Sand-molding (b) Metal-molding

Fig. 9. Fractographs of the combined tension and shear tests on the butterfly specimens with $\alpha = +10°$.

imposed by hydrostatic pressure (French and Weinrich, 1975; Biel-Golaska, 1998), and in combined tension and torsion tests (Barsoum and Faleskog, 2007).

The combined shear and compression tests give distinct fracture surfaces from the tensile tests. It can be seen from Fig. 10 that dimples are much smaller and shallower under shear than under tension. The fracture surfaces are relatively smooth. As the compressive stress increases, the void sheeting mode becomes dominant, see Figs. 11 and 12. In contrast to the cracking of particles in the tensile tests, silicon particles seem to be debonded from the matrix in these cases. This failure pattern was clearly demonstrated by Mohr and Treitler

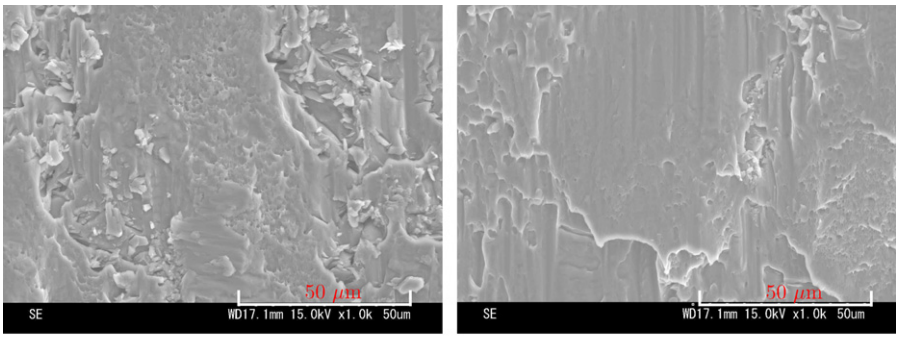

(a) Sand-molding (b) Metal-molding

Fig. 10. Fractographs of the simple shear tests on the butterfly specimens.

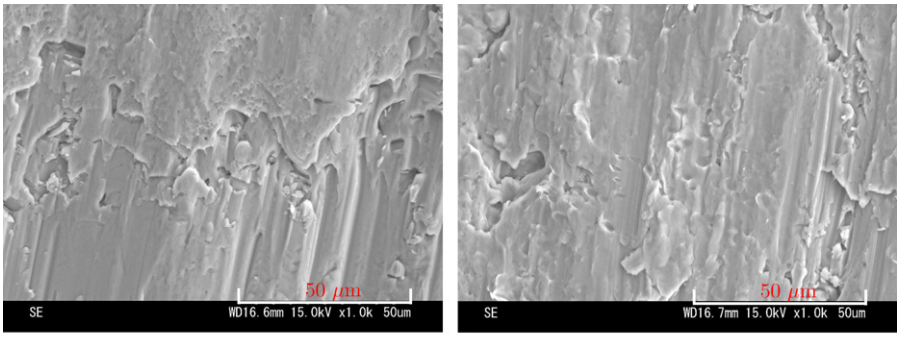

(a) Sand-molding (b) Metal-molding

Fig. 11. Fractographs of the combined compression and shear tests on the butterfly specimens with $\alpha = -5°$.

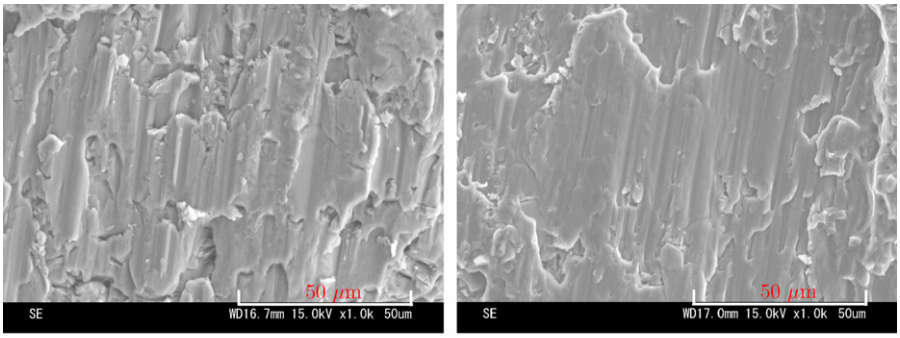

(a) Sand-molding (b) Metal-molding

Fig. 12. Fractographs of the combined compression and shear tests on the butterfly specimens with $\alpha = -10°$.

(2008) by polishing fracture sections. However, it is not clear how cracks developed between primary voids leading to the relatively smooth fracture surface. Compared to the tensile failure, the fracture mechanism under shear and compression is less understood. The problem needs to be further explored.

As far as effects of mold media are concerned, the two types of the casting specimens in general fail by the same mechanisms at the microscopic level. Since the sand-molding components are of large silicon particles, the round bars fail in a cleavage-like fracture way and the dimple microstructure is not easily identified. Under combined compression and shear, the fracture surface of the sand-molding specimens are relatively rough.

4. Plasticity and fracture properties

4.1. Load–displacement response

The difference in the material microstructure leads to various plastic deformation and failure response between the sand-molding and the metal-molding components. Figs. 13–15 show the load–displacement curves obtained from the tensile tests on the round bars and the biaxial loading tests on the butterfly specimens. It can be

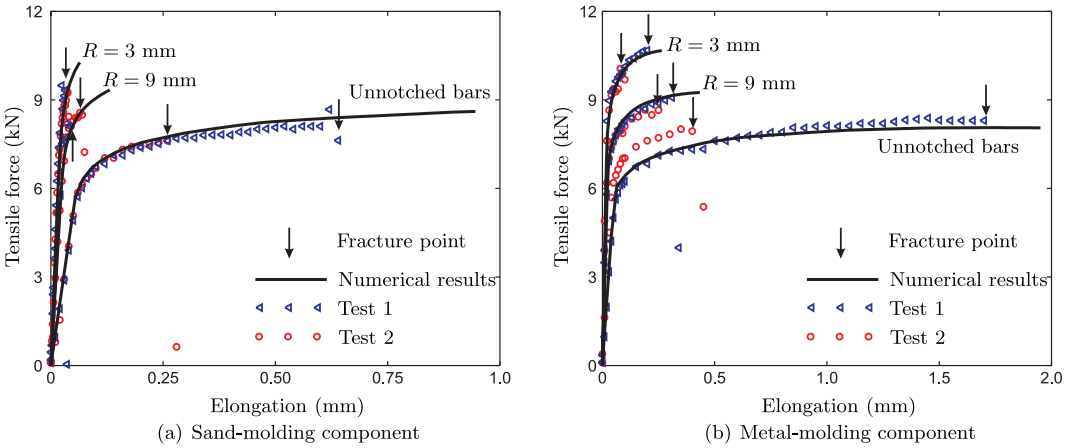

Fig. 13. The load–displacement curves obtained from the tensile tests on the notched and unnotched round bars machined from the sand-molding and the metal-molding components. The elongation is the relative displacement of the gauge section. The length of the gauge section is 20 mm, 10.64 mm, and 5.44 mm, respectively, for the unnotched bar and the notched bars of $R = 9$ mm and $R = 3$ mm.

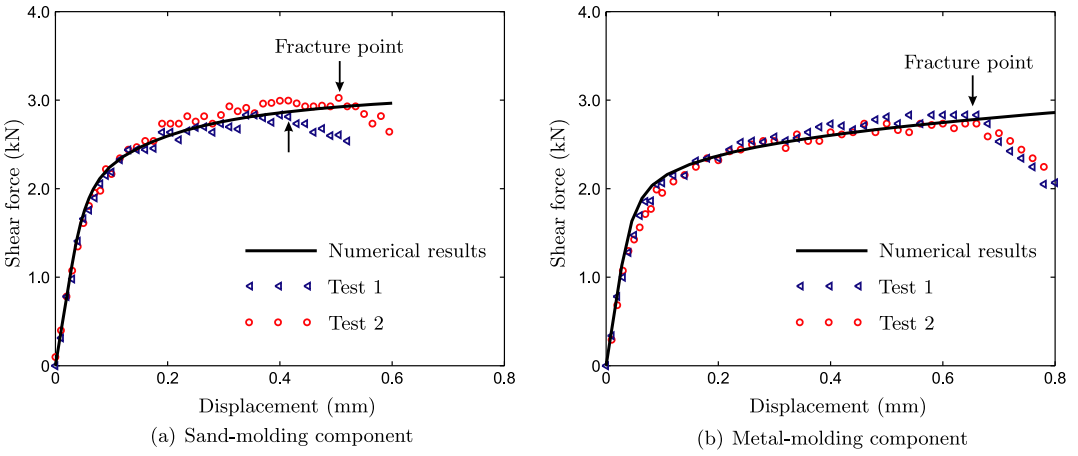

Fig. 14. The load–displacement curves obtained from the shear tests on the butterfly specimens machined from the sand-molding and the metal-molding components. The horizontal axis is the relative vertical displacement of the gauge section, which is of the length 3.0 mm.

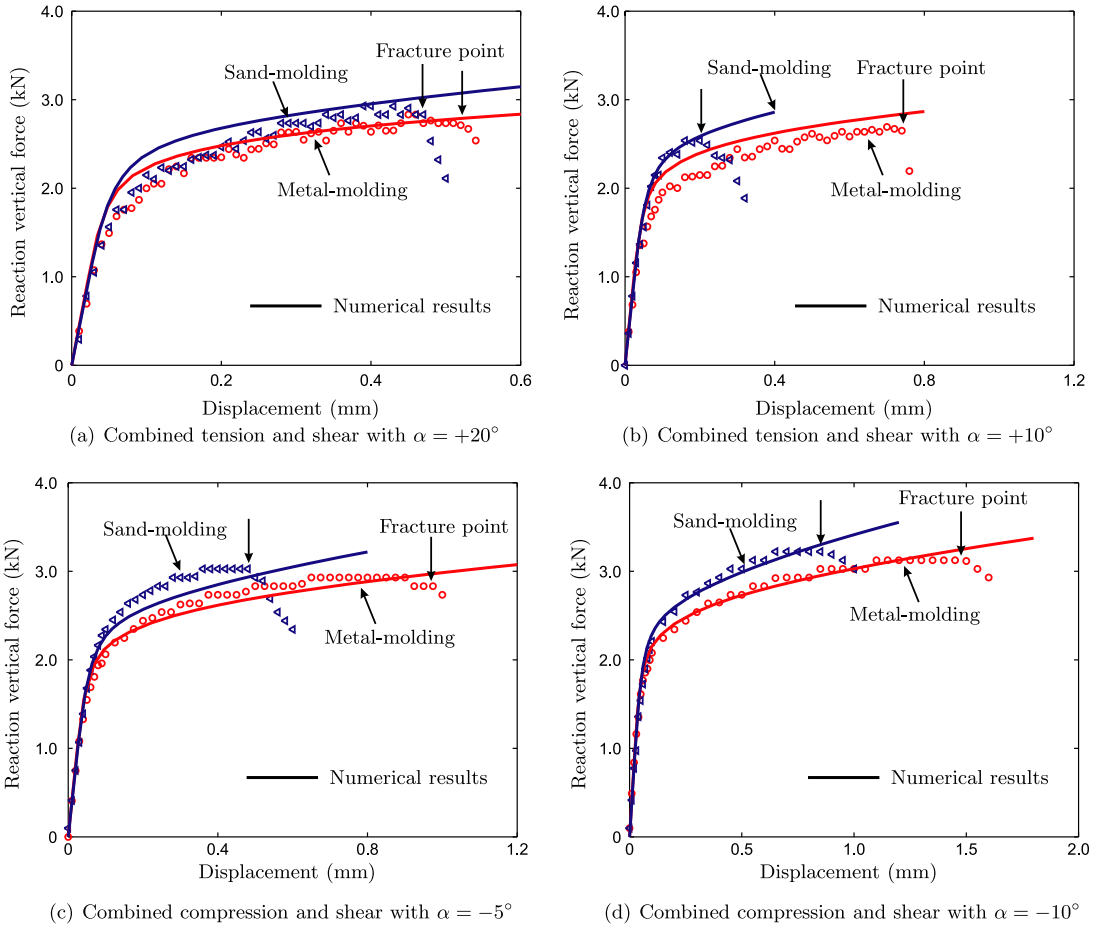

Fig. 15. The load–displacement curves obtained from the biaxial loading tests on the butterfly specimens machined from the sand-molding and the metal-molding components. The horizontal axis is the relative vertical displacement of the gauge section, which is of the length 3 mm.

clearly observed that at the same prescribed displacement the sand-molding specimens provide higher resistance than the metal-molding ones but fail earlier with the smaller critical displacements to fracture.

In the round bar tensile tests, the reaction forces suddenly drop to zero from the peak. The specimens were immediately broken into two pieces without evident signs of necking deformation. Based on a series of well-controlled fracture experiments, Bluhm and Morrissey (1965) concluded that this sudden drop corresponded to the formation of macroscopic cracks. By contrast, in the biaxial loading tests on the butterfly specimens the reaction forces gradually decrease after reaching the maximum value. To determine the instant of crack formation, some of the tests were purposefully stopped as soon as the load drop was noticed. One or several cracks can always be found on the exterior surface of the gauge section. Hence, the peak of the load–displacement curve of the biaxial loading test indicates the onset of macroscopic fracture. The instants of fracture are marked by the vertical arrows in Figs. 14 and 15, and used to calibrate the fracture loci of the two types of the cast aluminum components.

To examine experimental repeatability of the cast components, the tensile tests on the three types of round bars and the shear tests on the butterfly specimens were performed twice in this research. It appears from Figs. 13 and 14 that the load–displacement curves are generally close to each other but there is a certain variation in the fracture displacement. The scatter may be due to random distribution of defects such as gas and solidification pores. A statistical study of plasticity and fracture properties of cast aluminum components has been conducted. The results will be presented in a separate publication (Teng et al., submitted for publication).

4.2. True stress–strain curves

The difference in the load–displacement response between the sand-molding and the metal-molding castings can be clearly attributed to the distinction in plasticity properties. Fig. 16 illustrates the true stress–strain curves calibrated for the two types of the cast components. It appears that the sand-molding component is of higher yield resistance and hardening rate than the metal-molding one. This finding is consistent with the experimental data obtained by Wang (2003).

An inverse engineering approach was used to determine the true stress–strain curves. Two-dimensional, axisymmetrical and three-dimensional finite element models were developed, respectively, for the round bars and the butterfly specimens with ABAQUS/Standard. All the tests were numerically simulated to determine stress and strain. The interested reader can be referred to a previous paper by the same authors for details on the finite element procedure (Mae et al., 2007). As shown in Figs. 13–15, the numerically predicted load–displacement curves are generally in good agreement with the experimental results. This indicates that the stress–strain curves are correctly calibrated for the two types of the cast components. Slight discrepancies exist in some cases. Note, that the specimens were cut from different locations of the castings and may solidify at various rates. A recent statistical study of fracture tests on 30 identical casting specimens reveals that the variation of the load–displacement response can reach about 10% (Teng et al., submitted for publication).

4.3. Ductile fracture loci

To further distinguish effects of mold media, the ductility of the two types of the cast aluminum components is characterized from the preceding fracture tests. The ductility is understood as an intrinsic ability of a material to undergo a certain amount of plastic deformation without the occurrence of macroscopic cracks. A number of fracture criteria have been developed in the literature to describe the ductility. Wierzbicki et al. (Bao and Wierzbicki, 2004; Wierzbicki et al., 2005a; Teng and Wierzbicki, 2006) critically examined seven ductile fracture models commonly adopted in practical applications. They pointed out that a fracture locus formulated in the space of the effective plastic strain to fracture and the stress triaxiality would be the most suitable for a variety of problems. A general form of this type of fracture loci can be written as

$$\bar{\varepsilon}_{\mathrm{f}} = f(\eta) = f\left(\frac{\sigma_{\mathrm{m}}}{\bar{\sigma}}\right), \tag{1}$$

where $\bar{\varepsilon}_{\mathrm{f}}$ is the effective plastic strain to fracture and η is the stress triaxiality defined by the ratio of the mean stress σ_{m} to the equivalent stress $\bar{\sigma}$. The major task of this section is to determine the explicit expressions of Eq. (1) for the two types of the castings.

The preceding fractographic analysis shows that depending on stress states two distinct failure mechanisms compete with each other. Under tension, the failure of the specimens is characterized by void growth and the

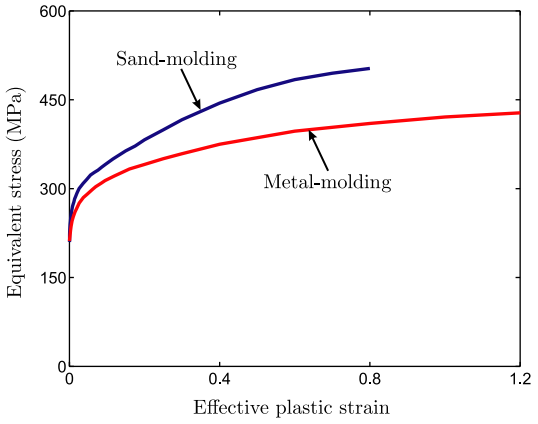

Fig. 16. The true stress–strain curves for the sand-molding and the metal-molding cast aluminum components. The elastic modula are $E = 82.0$ GPa and 86.0 GPa, respectively, for the sand-molding and the metal-molding components.

internal necking of the matrix. If compression is dominant, void sheeting due to shear is a preferable mechanism for crack formation. In the intermediate range, the specimens fail by the mixed mode. This clearly suggests that a fracture locus consist of three branches in the whole range of stress states. This type of fracture loci are developed for the two types of the castings.

In the range dominated by compression, Wierzbicki et al. (Wierzbicki and Werner, 1998; Bao and Wierzbicki, 2005) proposed that the fracture strain can be expressed by a hyperbolic function of the negative stress triaxiality:

$$\bar{\varepsilon}_f = \frac{C_1}{1+3\eta}, \quad -\frac{1}{3} \leqslant \eta \leqslant 0, \tag{2}$$

where C_1 is the material coefficient and is equal to the shear fracture strain, i.e. $C_1 = \bar{\varepsilon}_{f,s}$ at $\eta = 0$. As shown by Wierzbicki et al. (Wierzbicki and Werner, 1998; Bao and Wierzbicki, 2005), this fracture criterion is essentially equivalent to the ones suggested by Kudo and Aoi (1967), Cockcroft and Latham (1968), and Oh et al. (1979). They developed various fracture models by performing a series of upsetting tests on short cylinders. Bao (2003) examined the fracture surface of a cylinder in the upsetting test, which is quite similar to the one shown in Fig. 15(d). This indicates that the butterfly specimens under combined compression and shear fail by the same mechanism as cylinders in the upsetting tests. The similarity also justifies the use of Eq. (2) to characterize the fracture properties of the butterfly specimens under compression.

In the range of high positive stress triaxialities, an exponential function is widely used to describe the effective plastic strain to fracture:

$$\bar{\varepsilon}_f = C_2 \exp(C_3\eta) + C_4, \quad \frac{1}{3} \leqslant \eta, \tag{3}$$

where C_2, C_3, and C_4 are three material coefficients and need to be determined from tests. This functional form was first developed by Rice and Tracey (1969) by studying the enlargement of a spherical void embedded in a plastic matrix under hydrostatic tension, in which $C_3 = -1.5$ and $C_4 = 0.0$ were determined theoretically and C_2 is left for calibration. The applicability of Eq. (3) has been checked by a number of round bar fracture tests on various metals, e.g. Hancock and Mackenzie (1976) and Johnson and Cook (1985). The exponential function always gives an excellent fit to experimental data.

In the intermediate range, a linear relationship between the effective fracture strain and the stress triaxiality is simply defined:

$$\bar{\varepsilon}_f = \bar{\varepsilon}_{f,t} + (\bar{\varepsilon}_{f,t} - \bar{\varepsilon}_{f,s})(3\eta - 1), \quad 0 \leqslant \eta \leqslant \frac{1}{3}, \tag{4}$$

where $\bar{\varepsilon}_{f,t}$ is the effective fracture strain under uniaxial tension with $\eta = +1/3$. Here it is assumed that the transition of the failure mechanisms occurs at $\eta = +1/3$ and $\eta = 0$, which correspond to uniaxial tension and pure shear, respectively.

Such a three-branch fracture locus was first developed by Bao and Wierzbicki (2004) based on a series of fracture experiments. A similar trend was also observed by Barsoum and Faleskog (2007), who conducted combined tension and torsion tests on a Weldox steel. A schematic representation of this type of fracture models is given in Fig. 17.

The present formulation leaves four parameters to be calibrated from the fracture tests. Here a combined experimental–numerical approach is used. The finite element analysis provides the evolution of stress and strain states at each material point. The instants at fracture were determined from the tests in the form of the critical displacement of the gauge section to fracture.

In the round bar tensile tests, fracture usually initiates at the center of the necking zone due to high stress triaxialities. For the biaxial loading tests on the butterfly specimens, the cracks first occur in the middle thickness of the gauge section. These material points are identified as the critical sites for the onset of fracture. Their stress and strain states are used to determine the fracture locus. Fig. 18 shows the evolution of the stress triaxiality and the effective plastic strain of the critical points. It appears that the stress triaxialities vary in a rather narrow range in most of the tests. Hence, one can describe the stress state of each test using the average value of the stress triaxiality, defined by

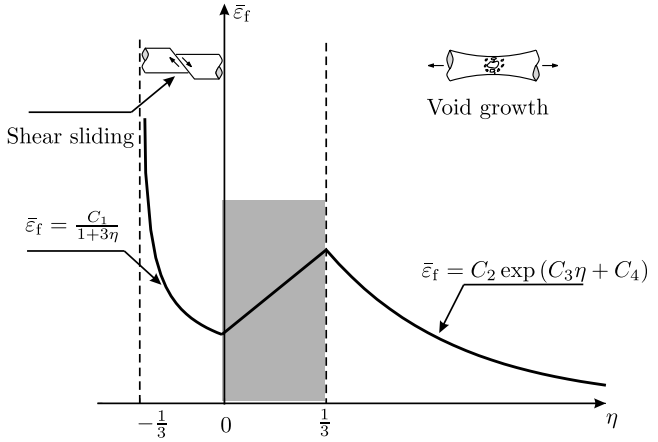

Fig. 17. Schematic representation of the three-branch fracture locus.

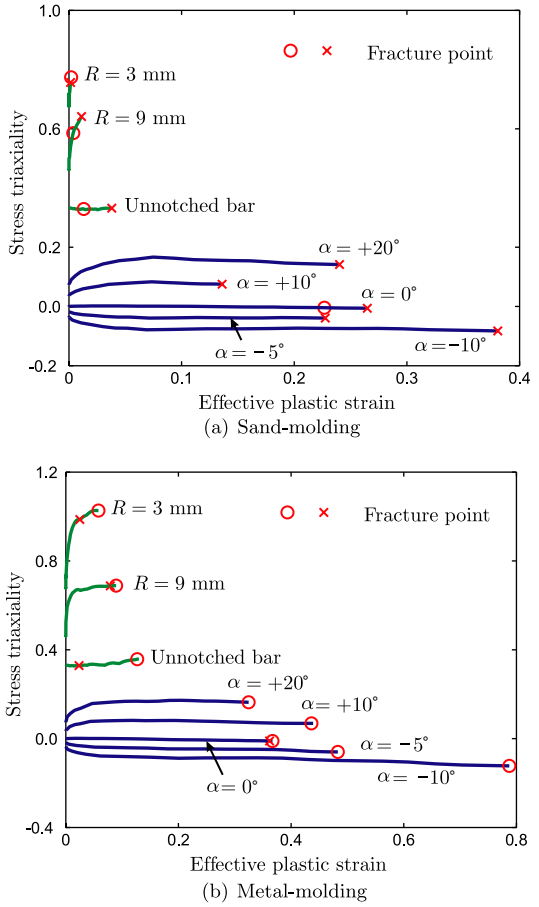

Fig. 18. Evolution of the stress triaxiality and the effective plastic strain of the critical material points for the specimens cut from the sand-molding and the metal-molding components.

$$(\eta)_{av} = \frac{1}{\bar{\varepsilon}_f} \int_0^{\bar{\varepsilon}_f} \eta \, d\bar{\varepsilon}_{pl}, \tag{5}$$

where $\bar{\varepsilon}_{pl}$ is the effective plastic strain.

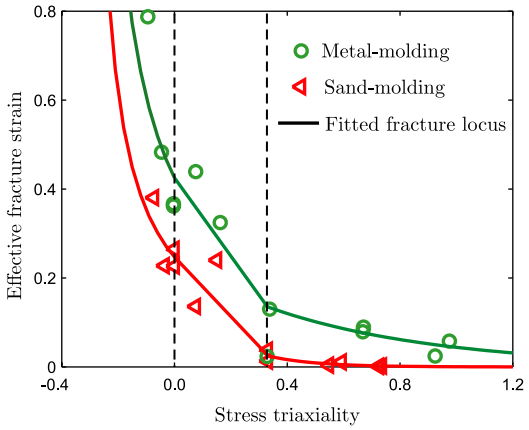

Fig. 19. Fitted three-branch fracture loci for the sand-molding and the metal-molding components. In curve-fitting, one point for the unnotched metal-molding round bar was discarded because of the abnormally small fracture strain.

Table 2
Material coefficients of the fracture loci for the two types of the castings

	C_1	C_2	C_3	C_4
Sand molding	0.247	0.176	5.915	0.0
Metal molding	0.425	0.235	1.672	0.0

Each test provides a point in the space of the average stress triaxiality and the effective fracture strain, see Fig. 19. C_1 is optimized from the four biaxial loading tests on the butterfly specimens. The other three coefficients are determined from the six tensile tests on the round bars. Table 2 lists the detailed values of the four parameters for the two types of the castings. It appears from Fig. 19 that the material ductility sharply decreases with the increasing stress triaxiality. For example, the effective fracture strain reaches 0.8 in the case dominated by compression while the effective fracture strain is as low as 0.13 in the round bar tensile tests for the metal-molding specimens.

In contrast to the fracture locus illustrated in Fig. 17, there is no distinctive "spike" in Fig. 19. For the present castings the effective fracture strain under shear is much higher than under uniaxial and thus the fracture loci appear to be much smooth.

Fig. 19 clearly demonstrates that the metal-molding component is of higher ductility than the sand-molding one. This indicates that one would be able to improve the ductility of castings by refining the microstructure. The finding is consistent with experimental results in the literature, e.g. Shabestari and Moemeni (2004).

5. Conclusions

The present paper studies the mechanical properties of the two types of the cast aluminum components using the combined experimental–numerical approach. The castings were made in sand molds and cast iron molds, respectively. A comparison was made to investigate the effect of the solidification rate on the plasticity and ductility.

Six notched and unnotched round bars and 6 butterfly specimens were prepared from each type of the castings. All the specimens were tested to fracture under a wide range of stress states including pure tension, combined tension and shear, pure shear, and combined shear and compression. To describe the plasticity and ductility of the castings, the true stress–strain curve and the fracture locus are calibrated, respectively, from the experimental data in combination with the finite element analysis. By comparing the curves, it can be readily seen that the metal-molding component is of lower yield resistance and higher ductility than the sand-molding one. Hence by increasing the solidification rate, one can improve the fracture property of castings.

The fracture surface of the specimens are examined using a scanning electron microscope. Two distinct fracture patterns are observed. In the tensile tests, fracture first occurs at large silicon particles by the cleavage mechanism. Cracks grow along grain boundaries leading to the complete failure of the round bars. The fracture surfaces are characterized by a number of dimples. By contrast, fracture is initiated by the debonding of the interface between the matrix and large particles if compression is dominant. Cracks are developed between primary voids due to void sheeting, which gives rise to the relatively smooth fracture surfaces. In the intermediate range of the stress triaxiality, two failure mechanisms compete with each other. The fractographic analysis suggests that the ductile fracture locus formulated in the space of the stress triaxiality and the effective plastic strain to fracture consist of three branches rather than a monotonic curve. Such a fracture locus is developed for the two types of the castings.

References

Bao, Y., 2003. Prediction of ductile crack formation in uncracked bodies. Ph.D. Thesis, Massachusetts Institute of Technology, Cambridge, MA, USA.

Bao, Y., Wierzbicki, T., 2004. A comparative study on various ductile crack formation criteria. Journal of Engineering Materials and Technology 126 (3), 314–324.

Bao, Y., Wierzbicki, T., 2004. On fracture locus in the equivalent strain and stress triaxiality space. International Journal of Mechanical Sciences 46 (1), 81–98.

Bao, Y., Wierzbicki, T., 2005. On the cut-off value of negative triaxiality for fracture. Engineering Fracture Mechanics 72 (7), 1049–1069.

Barsoum, I., Faleskog, J., 2007. Rupture mechanisms in combined tension and shear-Experiments. International Journal of Solids and Structures 44, 1768–1786.

Biel-Golaska, M., 1998. Analysis of cast steel fracture mechanisms for different states of stress. Fatigue and Fracture of Engineering Materials and Structures 21, 965–975.

Bluhm, J.I., Morrissey, R.J., 1965. Fracture in a tensile specimen. In: Yokobori, T., Kawasaki, T., Swedlow, J.L. (Eds.), Proceedings of the First Conference on Fracture, vol. 3, Sendai, Japan, September 1965, pp. 1739–1780.

Cáceres, C.H., Davidson, C.J., Griffiths, J.R., 1995. The deformation and fracture behaviour of an Al–Si–Mg casting alloy. Materials Science and Engineering A 197, 171–179.

Cockcroft, M.G., Latham, D.J., 1968. Ductility and the workability of metals. Journal of the Institute of Metals 96, 33–39.

Dighe, M.D., Gokhale, A.M., Horstemeyer, M.F., 2002. Effect of loading condition and stress state on damage evolution of silicon particles in an Al–Si–Mg-base cast alloy. Metallurgical and Materials Transactions A 33, 555–565.

French, I.E., Weinrich, P.F., 1975. The influence of hydrostatic pressure on the tensile deformation and fracture of copper. Metallurgical Transactions A 6, 785–790.

Hancock, J.W., Mackenzie, A.C., 1976. On the mechanisms of ductile failure in high strength steels subjected to multi-axial stress-states. Journal of the Mechanics and Physics of Solids 24, 147–169.

Johnson, G.R., Cook, W.H., 1985. Fracture characteristics of three metals subjected to various strains, strain rates, temperatures and pressures. Engineering Fracture Mechanics 21 (1), 31–48.

Kudo, H., Aoi, K., 1967. Effect of compression test conditions upon fracturing of medium carbon steel. Journal of Japanese Society of Technology and Plasticity 8, 17–27.

Leupp, J., Epprecht, W., 1977. Ductile intergranular fracture of an aluminium cast alloy. Scripta Metallurgica 11, 13–15.

Mae, H., Teng, X., Bai, Y., Wierzbicki, T., 2007. Calibration of ductile fracture properties of a cast aluminum alloy. Materials Science and Engineering A 459 (1–2), 156–166.

Mohr, D., Doyoyo, M., 2004. Experimental investigation on the plasticity of hexagonal aluminum honeycomb under multiaxial loading. Journal of Applied Mechanics 71, 375–385.

Mohr, D., Treitler, R., 2008. Onset of fracture in high pressure die casting aluminum alloys. Engineering Fracture Mechanics 75, 97–116.

Oh, S., Chen, C.C., Kobayashi, S., 1979. Ductile failure in axisymmetric extrusion and drawing Part 2: workability in extrusion and drawing. Journal of Engineering for Industry 101, 36–44.

Powell, G.W., 1994. The fractography of casting alloys. Materials Characterization 33, 275–293.

Rice, J.R., Tracey, D.M., 1969. On the ductile enlargement of voids in triaxial stress fields. Journal of the Mechanics and Physics of Solids 17, 201–217.

Rogers, H.C., 1960. The tensile fracture of ductile metals. Transactions of the Metallurgical Society of AIME 218, 498–506.

Shabestari, S.G., Moemeni, H., 2004. Effect of copper and solidification conditions on the microstructure and mechanical properties of Al–Si–Me alloys. Journal of Materials Processing Technology 153, 193–198.

Teng, X., Wierzbicki, T., 2006. Evaluation of six fracture models for high velocity perforation. Engineering Fracture Mechanics 73, 1653–1678.

Teng, X., Mae, H., Bai, Y., Wierzbicki, T., submitted for publication. Statistical analysis of ductile fracture properties of a cast aluminum alloy.

Wang, Q.G., 2003. Microstructural effects on the tensile and fracture behavior of aluminum casting alloys A356/357. Metallurgical and Materials Transactions A 34, 2887–2899.

Wierzbicki, T., Werner, H., 1998. Cockcroft and Latham revisited. Technical Report 16, Impact and Crashworthiness Lab, Massachusetts Institute of Technology, Cambridge, MA.

Wierzbicki, T., Bao, Y., Lee, Y.-W., Bai, Y., 2005a. Calibration and evaluation of seven fracture models. International Journal of Mechanical Sciences 47 (4–5), 719–743.

Wierzbicki, T., Bao, Y., Bai, Y., 2005b. A new experimental technique for constructing a fracture envelope of metals under multi-axial loading. In: Proceedings of the 2005 SEM Annual Conference and Exposition on Experimental and Applied Mechanics, pp. 1295–1303.